Hindawi
Journal of Chemistry
Volume 2022, Article ID 1961527, 12 pages
https://doi.org/10.1155/2022/1961527

Research Article

Recycling of Iron Slag Waste in the Production of Ceramic Roof Tiles

M. M. Ahmed,[1] **K. A. M. El Naggar**,[2] **M. F. Abadir**,[3] **W. Abbas**,[4] **and E. M. Abdel Hamid**[2]

[1]*Mathematics and Physics Engineering Department, Faculty of Engineering, Mataria, Helwan University, Cairo, Egypt*
[2]*Chemical Engineering Department, Egyptian Academy for Engineering and Advanced Technology (EAEAT), Cairo, Egypt*
[3]*Chemical Engineering Department, Faculty of Engineering, Cairo University, Cairo, Egypt*
[4]*Basic and Applied Science Department, College of Engineering and Technology, Arab Academy for Science, Technology and Maritime Transport, Cairo, Egypt*

Correspondence should be addressed to E. M. Abdel Hamid; eman.mohamed@eaeat.edu.eg

Received 22 March 2022; Revised 23 June 2022; Accepted 9 July 2022; Published 11 August 2022

Academic Editor: Ajaya Kumar Singh

The merit of this study is manufacturing cheaper roof tiles using fluxed waste material such as granulated iron slag, in addition to the environmental benefit of decreasing the cost and negative impact of their disposal and landfilling. Waste water-cooled granulated iron slag was ground and added in proportions ranging from 0 to 30 wt.% to kaolin clay to prepare roof tiles for the economic purpose of decreasing the production cost by incorporating cheap waste and to serve sustainability. The raw materials were characterized by XRD, XRF, and particle size analysis. The specimens were shaped using a rectangular mould with dimensions of $150 \times 30 \times 30\ mm^3$ under an axial pressure of 10 MPa and then dried in a dryer at 110°C. The firing of the dried specimens was carried out at 900, 1000, and 1100°C. The characteristics of fired specimens were determined by their linear firing shrinkage, water absorption, compressive strength, and freezing-thawing resistance. Results showed that samples containing 20% slag waste and fired at 1000°C displayed a cold water absorption of 12% and a saturation coefficient of 0.82, both values being lower than the maximum value recommended by standards. Also, the recorded breaking strength of 5040 N was much higher than the minimum standard value. These samples were also subjected to 50 freeze-thawing cycles, which they passed without the appearance of any cracks. It was concluded that samples containing 20% slag waste and fired to 1000°C or 1100°C fulfilled the requisites of ASTM C1167 for grade 3 normal duty roof tiles.

1. Introduction

In the last few decades, the use of clay roof tiles has been boosted by the stringent restrictions put on the use of asbestos as a roofing material owing to its harmful health effects [1, 2]. Clay roof tiles are nowadays finding wide applications in traditional homes, hotels, or resort construction owing to their attractive appearance and properties such as high strength and high durability [3, 4]. The fact that such tiles need firing at elevated temperatures exceeding 1000°C has had, however, a negative impact on the economics of their production. This has prompted an investigation into the incorporation of various industrial wastes into the tile recipe to limit their manufacturing cost [5].

In this connection, many studies have been carried out to substitute part of the original clay mix with industrial refuse materials. Dondi et al. showed the possibility of using glass waste produced from PCs and TVs in the production of roof tiles. Glass waste (cullet) was crushed and ground to a particle size of less than 1 mm. Specimens were prepared by mixing clay with different percentages ranging from 0 to 5% wt. of waste, to be then shaped by plastic extrusion, dried, and fired at different firing temperatures (900, 950, and 1000°C), with a soaking time of 4 hours. The characteristics of the produced roof tiles were determined, such as water

absorption, open porosity, bulk density, and modulus of rupture. The authors concluded that it was possible to substitute the original clay mix by up to 4% without impairing the properties of the fired bricks [6]. On the other hand, Gaggino et al. investigated the addition of rubber and plastic waste in the preparation of roof tiles. Their results indicated that adding these wastes enhanced the physic mechanical properties of the tiles by decreasing porosity and increasing flexural strength [7]. Using rock dust as an additive, Sultana et al. investigated the effect of that addition on the properties of fired roof tiles. They mixed red clay with different percentages of rock ranging from 10% to 50% and sintered the produced mixes at temperatures ranging from 850 to 1100°C. They concluded that it was possible to reach a flexural strength of about 32 MPa with water absorption of 6.5% by adding 40% waste and firing at 900°C [8]. In a different context, Ingunza et al. incorporated domestic sewage sludge into the manufacturing of ceramic roof tiles. Five mixtures were prepared using different proportions of sludge ranging from 2% to 10% by weight as a partial replacement for clay. Because of the high organic matter content in the sludge (>70%), the addition was limited to 4% by weight so as not to negatively affect water absorption and flexural strength [9]. On the other hand, De Silva et al. studied the possibility of replacing clay with rice husk ash (RHA) in the preparation of ceramic roof tiles. They fired specimens with different compositions ranging from 0% to 20% of waste substitution at temperatures reaching 1100°C. They determined the effect of waste addition on water absorption and flexural rupture strength and found a replacement of 10% wt. increased the breaking load by about 45.97% due to high ductility compared to the standard tiles. They concluded that RHA can replace clay up to 15% to satisfy the limit of water absorption imposed by standards [10]. Using a mixture of coal fly ash and tile waste to partly substitute clay in roof tile recipes, Figen et al. investigated three different types of ash and found out that the maximum possible level of addition depended on the chemical analysis of the ash used. A mix containing 5% tile waste and two different types of fly ash could be used to produce good quality tiles by firing at 1000°C [11]. Recently, Khater et al. [12] were able to produce porous ceramic tiles by using two waste materials, namely arc furnace sludge, and ceramic sludge. Their work concentrated on the electric properties of the produced bodies, whereby their samples proved to have low electrical conductivity and could therefore be used as electrical insulators.

In connection to the present work, the use of metallurgical slags in the preparation of roof tiles was tackled by a limited number of authors. Kallas et al. [13] discussed the feasibility of the incorporation of nickel slag as secondary raw material in the manufacturing of roof tiles. They mixed the basic mixture of roof tiles with different percentages of waste to determine the optimum composition. They found that slag waste could be used up to 25% in roof tiles to meet Brazilian Technical Standards. The addition of nickel slag waste increased the density and mechanical strength but reduced the permeability and water absorption of the tiles. Amin et al. [14] studied the effect of using marble dust as secondary raw material in the manufacturing of roof tiles. They characterized the marble dust and the basic raw materials used for ceramic tiles using XRF and XRD. They prepared mixtures with different compositions of waste ranging from 0% to 30% by weight as a partial replacement of the standard mix of roof tiles. This was followed by moulding, drying, and firing at temperatures ranging from 1000°C to 1150°C with a soaking time of 3 hours. They determined the physical and chemical properties of the produced roof tiles as compared to standard values. They found marble dust can be used in roof tiles up to a 10% addition and firing temperature at 1000°C. Also, Lemougna et al. [15] suggested the use of copper smelting slag to prepare structural ceramic components, including roof tiles. They claimed a compressive strength of 140 MPa for the prepared components and interpreted their findings by XRD investigation. It is believed that the exaggerated value of compressive strength was due to the small sample size ($20 \times 20 \times 20\ mm^3$). On the other hand, Ahmed et al. [16] recently investigated the possibility of using aluminium smelting slag in the preparation of clay roof tiles. Their results revealed that it was possible to obtain tiles abiding by standards by the substitution of clay with 40% slag and firing at 1100°C. The addition of sulfidic mine tailings in the preparation of roof tiles was recently researched by Paiva et al. [17], who could reduce the firing temperature from 1150°C to 1050°C by adding 20% tailings to a standard mix. As for the use of iron slag, this was the topic of research investigated by Ghosh et al. [18] for ceramic tiles rather than roof tiles. They obtained water absorption figures as low as 2.5% and flexural strengths ranging from 28 to 38 MPa. The closest to the present work is that reported by Kim et al. [19], who prepared roof tiles by mixing clayey materials (79.5%) with 15% ferronickel slag with the balance magnesium aluminium silicate. Upon firing at 1125°C, the produced bricks showed a breaking strength of 12 kN and cold-water absorption of 6.08%.

In the present work, the use of Granulated Blast Furnace Slag (GBFS) waste as a partial substitute for the original clay mix is investigated for the dual purpose of managing waste and obtaining lower-cost roof tiles as per ASTM C1167 [20]. The main reason for using that particular type of slag is to make use of the fluxing oxides present in that slag, which can potentially reduce the firing temperature of the tiles, which normally ranges from 1100°C to 1200°C [21]. To the authors' knowledge, there were no previous trials to incorporate blast furnace slag into the recipe for clay roof tiles.

2. Materials and Methodology

The present section deals with the type of raw materials used, their source, and the methods used for characterization. This is followed by a brief description of the method of preparation of samples and the methods used for determining the properties of both dry and fired samples.

2.1. Raw Materials. The raw materials used in the study were Aswan kaolin clay (Upper Egypt) and ground granulated blast furnace slag (GBFS). Kaolin clay was crushed and

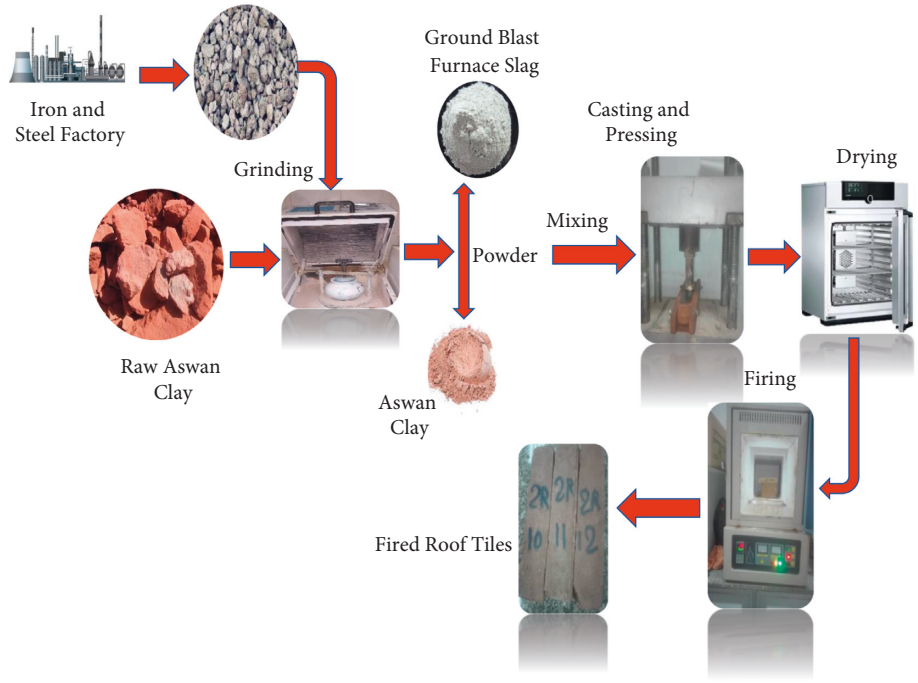

Figure 1: Experimental procedure.

ground, while ground granulated blast furnace slag (GBFS) was obtained from the Iron and Steel Factory,Helwan, Egypt. Both raw materials were characterized through the following techniques:

Chemical composition was determined using X-ray fluorescence (XRF) that was run on an AXIOS, Panalytical 2005, Wavelength Dispersive (WD–XRF) Sequential Spectrometer.

The mineralogical composition of both materials was determined by X-ray diffraction (XRD) using the Bruker D8 advanced computerized X-ray diffractometer apparatus with mono-chromatized CuKα radiation, operated at 40 kV and 40 mA.

Scan Electron Microscope (SEM) micrographs were obtained using a JEOL-JSM 6510 type microscope with a maximum magnification of 300,000.

The particle size distribution was determined using the standard sieve analysis procedure according to ASTM C136-01 [22].

2.2. Preparation of Roof Tile Samples. Three clay-slag mixtures were prepared by replacing clay with different percentages of GBFS: 0%, 10%, 15%, 20%, and 30% (by weight). Water was then gradually added in at a proportion of 20% to impart plasticity to the mix.

The different mixtures were shaped using rectangular moulds of dimensions ($150 \times 30 \times 30\ mm^3$) and then pressed by uniaxial pressing at 10 MPa. These dimensions were chosen to allow for determining the mechanical properties of flexural strength, while the uniaxial pressure used was enough to ensure proper consolidation of the samples before firing.

Green ceramic bodies were left in the air and then dried for 24 hours in a dryer at 110°C, after which the specimens were fired in a muffle furnace with a soaking time of 1 h at different temperatures (900°C, 1000°C, and 1100°C). After soaking, all specimens were allowed to cool naturally to the ambient temperature inside the furnace. The experimental procedures were shown in Figure 1.

2.3. Properties of Dry and Fired Samples. The properties of dried and fired samples will be discussed in the following section.

2.3.1. Linear Shrinkage (LDS and LFS). The linear drying shrinkage of the specimens (LDS) was determined using the following definition:

$$\text{LDS\%} = \frac{L_w - L_d}{L_w} \times 100, \quad (1)$$

where L_w and L_d are the wet and dry lengths, respectively.

Also, the linear firing shrinkage (LFS) was obtained using a similar following expression:

$$\text{LFS\%} = \frac{L_d - L_f}{L_d} \times 100, \quad (2)$$

where L_d and L_f are dry and fired lengths, respectively.

Both parameters (LDS and LFS) were determined following ASTM C326-09 [23].

2.3.2. Water Absorption (WA), Bulk Density, and Porosity. There are two standard tests for water absorption as regulated by ISO 10545 [24]. Coldwater absorption (CWA) and

boiling water absorption (BWA) are defined by the following relation:

$$\mathrm{WA} = \frac{m_w - m_d}{m_d} \times 100, \quad (3)$$

where m_d and m_w are the dry and wet masses, respectively.

The ratio between the values of CWA and BWA is termed the Saturation Coefficient (SC) and is indicative of the size of the pores. A high SC means that the pores are large enough to allow them to be filled by cold water since the resisting action of trapped air bubbles will be negligible. The standard ASTM C1167-11 (2017) [19] stipulates that this ratio should not exceed 0.86.

On the other hand, the bulk density of fired samples was calculated as the ratio between their mass and bulk volume, whereas the powder density was determined by the pycnometer method as regulated by ISO787-10 [25].

Also, the apparent porosity of the fired samples was determined following ISO787-10 [25] as being the ratio between the open pores of the specimen and its bulk volume. As for the total porosity, it was calculated from the values of bulk density (ρ_B) and powder density (ρ_P) through the following relation:

$$P\% = \left(1 - \frac{\rho_B}{\rho_P}\right) \times 100. \quad (4)$$

2.3.3. Transverse Breaking Strength (BS) and Modulus of Rupture (MOR). According to ASTM C1167-11 [21], the transverse breaking strength is determined using a three-point bending test. It is calculated from the following relation:

$$\mathrm{BS} = \frac{F.L}{b}, \quad (5)$$

where BS is the Breaking Strength (N), F is the braking load (N), L is the distance between the two supports (mm), and B is the breadth of the tile specimen.

The minimum allowable breaking strength for roofing clay tiles, following ASTM C1167-11, is 1334N.

The modulus of rupture (MOR), on the other hand, is not a standard requisite for clay roofing tiles. However, it was determined to follow the effect of percent GBFS substitution and firing temperature on the transversal flexural strength. Its value can be deduced from that of the breaking strength through the following formula:

$$\mathrm{MOR} = \frac{3.\mathrm{BS}}{2d^2} \cdot \mathrm{MPa}, \quad (6)$$

where d is the specimen thickness (mm).

2.3.4. Freezing-Thawing Resistance. Following ASTM C1167-11, five tile specimens should show no cracks or breakage after 50 freezing-thawing cycles.

Table 1: Chemical analysis of raw materials.

Component	Clay wt.%	GBFS wt.%
Al_2O_3	32.906	9.97
SiO_2	48.931	38.67
Na_2O	0.094	0.99
K_2O	0.014	0.53
CaO	0.505	34.02
MgO	0.09	4.11
TiO_2	5.918	0.62
Fe_2O_3	1.193	0.68
SO_3	0.291	2.68
Cl	0.011	0.04
Cr_2O_3	0.138	0.014
ZrO_2	0.465	0.081
LOI	9.2	2.74
Total	**99.756**	**99.654**

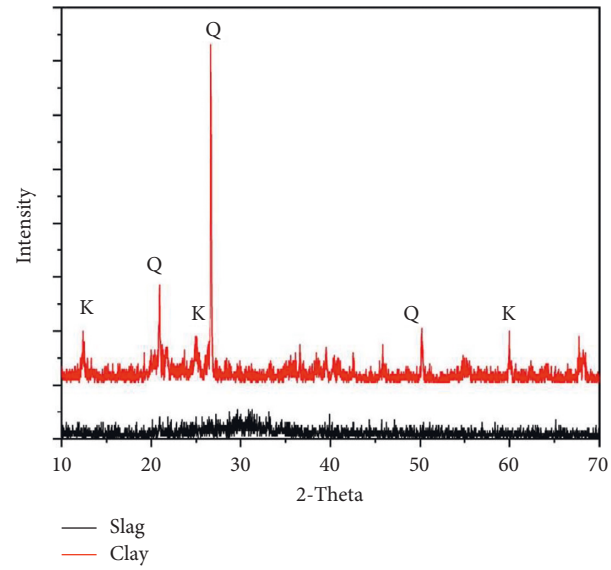

Figure 2: XRD patterns for clay and GBFs.

2.3.5. Reproducibility of Experimental Results. To ensure the reproducibility of results, a minimum of three specimens per sample were tested each time, the number raised to five whenever required by the relevant standard specification (ASTM C1167-03). The mean value was chosen each time, and Dixon's rule was used to reject possible outliers [26].

3. Results and Discussion

This section includes the results obtained for the chemical and mineralogical characterization of the raw materials, followed by the experimental results obtained for dry and fired samples.

3.1. Characterization of Raw Materials. The following section shows the characterization of raw materials.

3.1.1. Chemical Composition. Table 1 shows the chemical analyses of both clay and iron slag used in that work. As

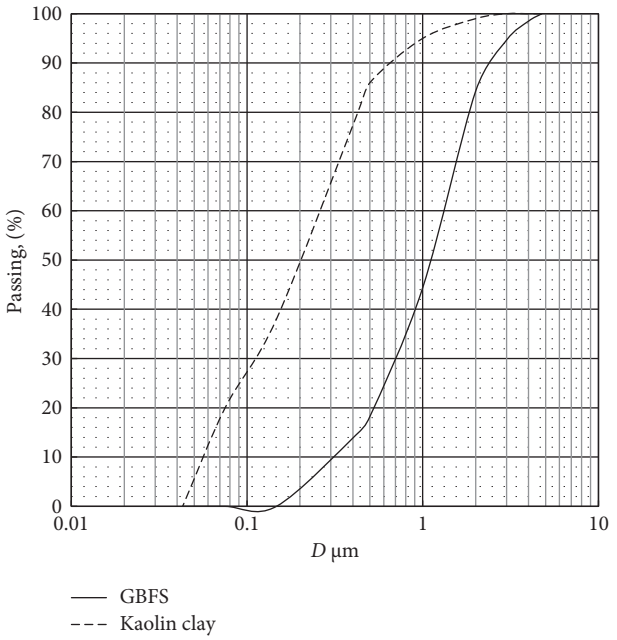

Figure 3: Particle size distribution of raw materials.

expected, while the predominant phases in clay are alumina and silica, these are calcium oxide and silica in the case of slag. The percent calcium oxide (34.02) % is typical, as reported by El-Chabib in his comprehensive review on the matter (32.6–43.9%) [27].

It also appears from that table that the loss on ignition of clay is 9.2% owing to the dehydroxylation of kaolin to metakaolin according to the following reaction [28]:

$$Al_2Si_2O_5(OH)_4 = Al_2O_3.2SiO_2 + 2H_2O. \quad (7)$$

As for the loss on ignition of slag (2.74%), this is presumably due to the decomposition of calcium hydroxide, carbonate, and bicarbonate that were formed on slaking by a reaction between any free oxide present and the surrounding atmosphere.

3.1.2. Mineralogical Composition. As established from XRD, the mineralogical composition of the raw materials is illustrated in Figure 2. This reveals that kaolin clay is mainly composed of kaolinite ($Al_2Si_2O_5(OH)_4$) and quartz (SiO_2), whereas slag is almost amorphous, although it exhibits a diffuse peak at 29–30° indicative of the presence of calcite ($CaCO_3$) formed by the slaking of free lime present in slag.

3.1.3. Particle Size Distribution. Figure 3 displays the particle size distribution of both raw materials. It appears from that figure that kaolin clay is much finer than ground slag. The median particle size (D_{50}) for kaolin is 0.2 mm, while that of ground slag is 1.1 mm.

3.1.4. Powder Densities of Raw Materials. The powder densities of both materials were determined using the pycnometer method. The powder density of kaolin clay = $2.62 \pm 0.05\ g{\cdot}cm^{-3}$ and that of GBFS = $2.86 \pm 0.08\ g{\cdot}cm^{-3}$.

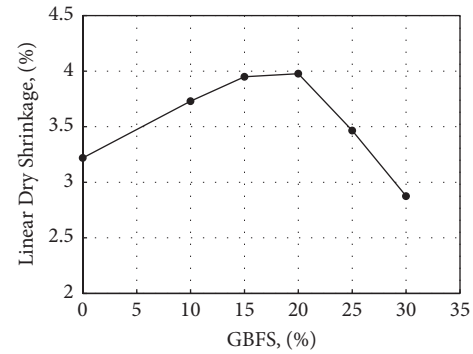

Figure 4: Effect of GBFS addition on Linear Drying Shrinkage.

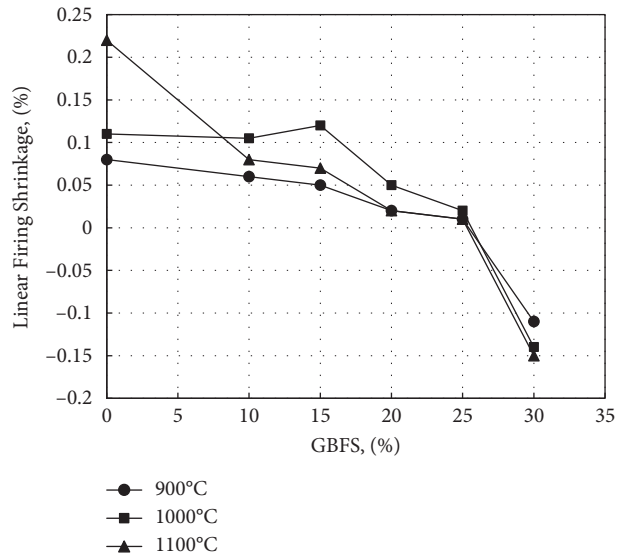

Figure 5: Effect of GBFS addition on linear firing shrinkage.

3.1.5. Determination of Free Lime in Slag. This was determined using the ethylene glycol method of McPherson and Forbrich as detailed by Goto and Kakita [29]. The test was repeated on three different specimens to obtain an average value of 2.128% CaO. Since all free lime will have been slaked to calcium carbonate, as evidenced by the obtained XRD results, the corresponding percentage of calcium carbonate would amount to about 4.07%. This figure is compatible with the findings of Vilciu et al. [30], who put the level of free CaO between 1.7 and 7%.

3.2. Results of Dry and Fired Samples. The experimental results of the dried and fired samples are discussed in the following sections.

3.2.1. Linear Drying Shrinkage (LDS). The addition of GBFS waste to kaolin resulted in a slight increase in LDS up to 20% addition, followed by a sharp drop for higher replacement

ratios. One possible reason is that the glassy nature of GBFS allows its particles to slide easily between the kaolin particles so that there is an initial increase in shrinkage on adding GBFS waste that does not practically vary as the percentage of slag moves from 10% to 20%. Above this level, however, the nonplastic nature of slag prevails, resulting in a decrease in drying shrinkage [31] (Figure 4).

3.2.2. Linear Firing Shrinkage (LFS). Figure 5 shows the results obtained for the effect of waste substitution for clay on the percent linear firing shrinkage. It appears from that figure that shrinkage decreases on adding GBFS waste to the extent that an increase in dimensions can be observed in samples containing more than 25% slag, as evidenced by the negative values of shrinkage. It has been observed that the highest firing shrinkage reached was at 1000 and 20% GBFS. Increasing the addition of GBFS was the cause of greater ultimate linear shrinkage which reached for the presence of greater amounts of CaO that decreased viscosity of glassy phase, the release of CO_2 from pores became easier and greater sintering was achieved [32]. This result complies with that obtained by Ozdemir and Yilmaz, who studied the effect of replacing blast furnace slag with clay [33]. The effect of releasing gases will be explained in terms of porosity changes in the water absorption and porosity.

3.2.3. Bulk Density. The dependence of the bulk density on the sintering temperature and percentage slag addition is plotted in Figure 6. The bulk density was increased by increasing temperature and slag replacement by up to 20%. The densification was improved with the additives due to the formation of glassy phases in grain boundaries, which causes viscosity reduction and faster particle growth, leading to greater crystals. The values of bulk density were less than those obtained by many preceding studies [32, 34, 35].

3.2.4. Water Absorption and Porosity. Figures 7–9 display the effect of percent GBFS used on cold water absorption (CWA), boiling water absorption (BWA), and Saturation Coefficient (SC), respectively. Firing at 900°C is not associated with much sintering, which results in the presence of large pores that impart to the samples a high saturation coefficient. As the firing temperature is increased, the pore sizes decrease, followed by a decrease in saturation coefficient. This is since an increase in temperature reduces the viscosity of slag as its softening temperature usually ranges from 1030°C to 1200°C [36]. This facilitates its flow into the pores, causing a corresponding decrease in pore size. The maximum value of saturation coefficient of 0.87, as regulated by ASTM C1167, appears only in samples containing 20% or 30% slag fired to 1000 or 1100°C.

On the other hand, minimum cold water absorption of 11.6% is achieved at about 20% addition for samples fired at 1100°C. A maximum percent cold water absorption of 13% as stipulated by ASTM C 1167, a condition fulfilled by samples containing between 15% and 25% GBFS and fired at 1000°C and 1100°C, which is comparable to the results obtained by

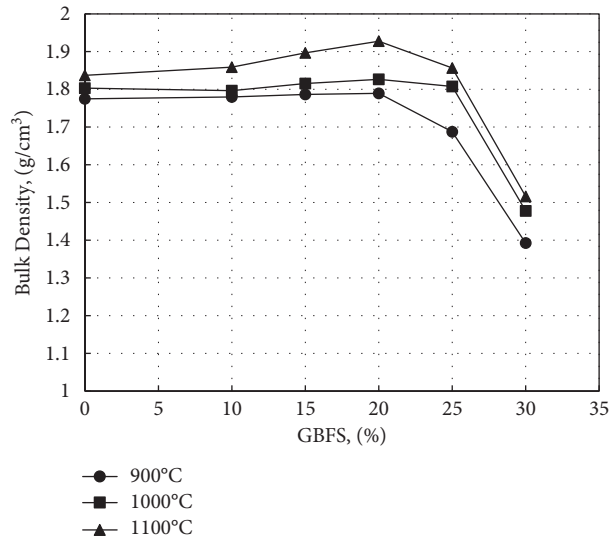

Figure 6: Variation of bulk density with different GBFS percentage.

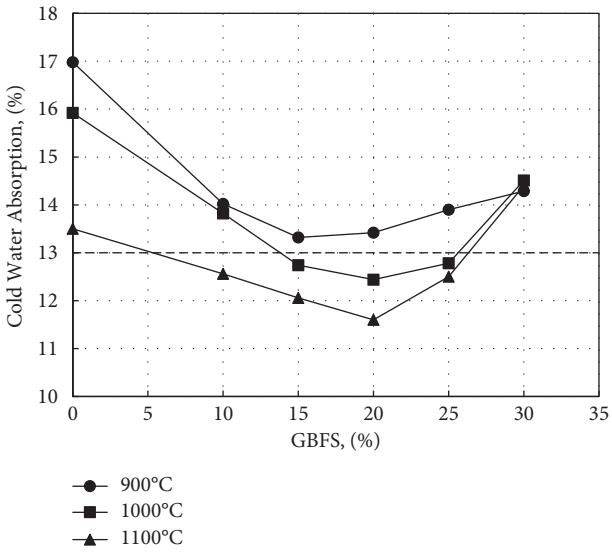

Figure 7: Effect of GBFS addition on cold water absorption. (Dotted line corresponds to maximum value following ASTM C1167).

Ozdemir and Yilmaz [33]. Any further increase in GBFS content over 20% has the effect of causing bloating of the samples, resulting in warping and the formation of surface cracks that increase water absorption. This is believed due to the expansion of pores following dehydroxylation of kaolinite. Aside from the decomposition of calcium carbonate formed by the slaking of free lime in slag, trapped gases in pores tend to expand. This expansion in dimensions accompanying warping is greatly facilitated by the increase in liquid phase content and explains the negative values of linear firing shrinkage observed in Figure 5 as the percent slag exceeds 20%. The minimum figure obtained for cold water absorption for samples fired at 1100°C (11.6%) is lower than that obtained by Ahmed et al. [16] on incorporating 40% aluminium slag in roof tile mixes (12.8%) and that of Kallas et al. [13] on adding

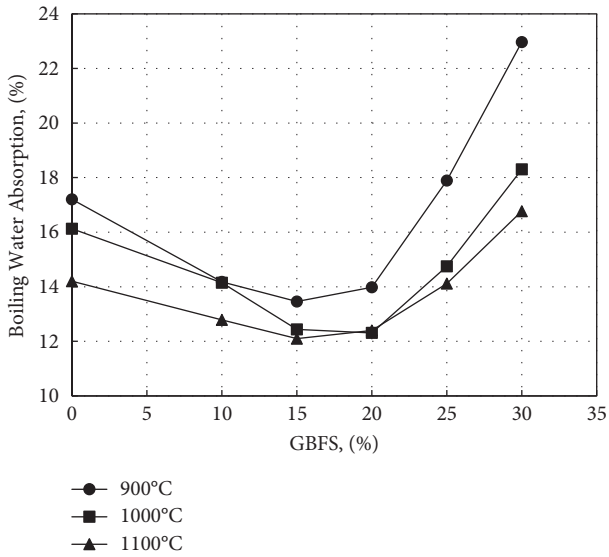

Figure 8: Effect of GBFS addition on boiling water absorption.

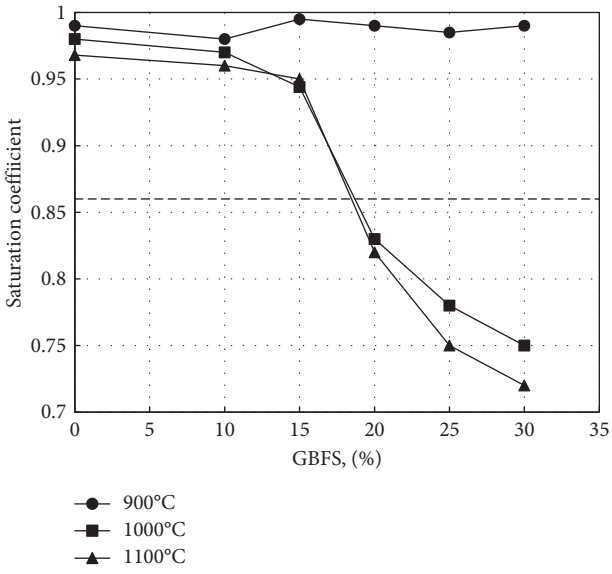

Figure 9: Effect of GBFS addition on saturation coefficient. (Dotted line corresponds to maximum value following ASTM C1167).

15% nickel slag (21%). While the values of saturation coefficient obtained in the present work for samples containing 20% GBFS fired at 1000 or 1100°C dropped to values lower than the maximum value of 0.87 [20], the corresponding values for aluminium slag were 0.95 and 0.88, respectively [16]. The present values of water absorption are, however, higher than those obtained by Kim et al. [19] by using 15% ferronickel slag and firing at 1125°C (6.03%). It is believed that the addition of 5.5% magnesium aluminium silicate to this mix has contributed to lowering the porosity by promoting the formation of a liquid phase.

The formation of the liquid phase is illustrated in Figure 10, in which two specimens fired at 1100°C and containing 20% and 30% GBFS, respectively, are pictured. Also,

Table 2: Effect of percent GBFS on number of freezing–thawing cycles with No cracks.

GBFS%	0	10	15	20	25	30
No of cycles before appearance of cracks	50	50	50	50	46	33

Figure 11 shows the SEM micrographs obtained for specimens containing 20% and 30% GBFS fired at 1100°C. As can be seen from this figure, the specimen containing 20% GBFS displays limited liquid phase formation, while the specimen with 30% GBFS shows the formation of large amounts of the liquid phase. This explains the increase in dimensions observed in Figure 3 due to bloating. This has the effect of causing warping and the appearance of cracks, as illustrated in Figure 10.

The fact that an increase in GBFS content from 20% to 30% causes an increase in liquid phase formation can be explained according to the SiO_2-Al_2O_3-CaO diagram shown in Figure 12. Upon firing, clay and GBFS lose their chemical water, as evidenced by the Loss on Ignition revealed in Table 1. Therefore, the percent of all oxides appearing in that table can be reduced to an ignition-free basis upon firing. Moreover, after this reduction, the percentages of the three oxides (SiO_2-Al_2O_3-CaO) will exceed 90%. As a first approximation, their composition can be reduced to a total of 100% by multiplying their percentages by 10/9. This way, the 20% and 30% mixtures will be represented on that diagram by points A and B, respectively. On that diagram, the initial melting points of the two compositions will be 1550°C and 1170°C, respectively, while the final melting points will be 1710°C and 1515°C, respectively. This reveals the effect of increasing the percent GBFS on the melting behaviour of the two mixes, as the second one will melt at a lower temperature than the first. It should be noted that the presence of other fluxing oxides such as K_2O, Na_2O, and Fe_2O_3 in the mixes will result in lowering the above-mentioned figures for temperatures.

The effect of waste addition on apparent porosity is displayed in Figure 13 and follows, as expected, the same trend of water absorption. The apparent porosity decreases with increasing GBFS till reaching 20%, with an apparent porosity of 21.3% at 1000°C and 19.6% at 1100°C. Then, above 20%, apparent porosity increases due to expansion of pores as a result of dehydroxylation of kaolinite besides the decomposition of calcium carbonate. On the other hand, it was possible to calculate the total porosity using equation (4) and deduce the closed porosity by subtracting the apparent porosity from its values. Figure 14 shows the variation of total and closed porosities for samples fired at 1000°C. It appears from this figure that there is an appreciable increase in closed porosity following sintering and vitrification as the slag level exceeds 20%, particularly for samples fired at 1000 or 1000°C.

3.2.5. Freeze-Thawing Resistance. Samples containing different percentages of GBFS fired at 1000°C were tested for freezing-thawing resistance. Table 2indicates the number of cycles after which cracks started to appear on the samples. Since a sample is considered to have passed the test if no

(a) (b)

Figure 10: Specimens fired at 1000°C and containing different percentages of GBFS. (a) 20% slag; (b) 30% slag.

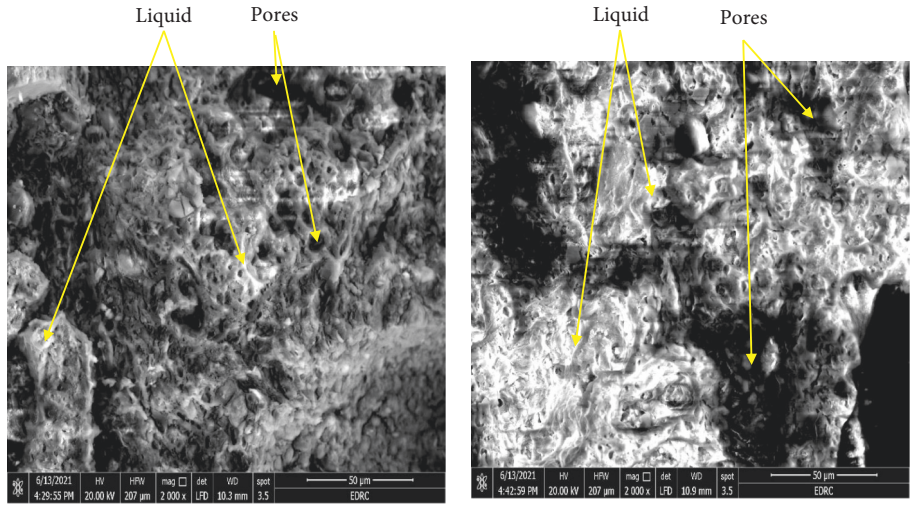

(a) and (b)

Figure 11: Sem micrographs for specimens fired at 1000°C containing (a) 20% GBFS and (b) 30% GBFS.

cracks appear after 50 cycles, it can be concluded that the maximum percent GBFS addition without freeze-thawing failure is 20%.

3.2.6. Mechanical Properties. Figure 15 illustrates the effect of GBFS substitution for clay on the transverse breaking strength. The dotted line in the figure corresponds to the minimum value of 1334°N required by the standard ASTM C1167-03. As shown, except for some samples fired at 900°C, this value is largely exceeded on firing at 1000°C and 1100°C. Reached 5050°N and 7000°N, respectively, for samples containing 20% GBFS, which is much higher than that obtained by replacing aluminium slag with the same type of clay [16]. However, it appears from the results obtained at these two firing temperatures that a drop in strength takes place as the percent slag content exceeds 20%. This is presumably due to crack formation and an increase in total porosity, as can be seen in Figure 13. These values are lower than those obtained by Kim et al. [19] for samples containing 15% ferronickel slag and 5.5% aluminium magnesium silicate fired at 1125°C (12100°N). In any case, the minimum required breaking strength is largely exceeded, and it is believed that the production economics of roof tiles using the additions made by Kim et al. [19] may not be viable. This is since aluminium magnesium silicate has to be prepared synthetically and therefore cannot be regarded as cheap waste.

As observed from Figure 16, the curves of MOR follow a more or less similar pattern, producing maximum values of MOR of 11.3 MPa for samples containing 20% GBFS fired at 1000°C and 15.4 Mpa for samples containing 15% slag fired at 1100°C. A comparison of MOR values with those obtained by Kallas et al. [13] and Ahmed et al. [16] who used nickel and aluminium slags respectively in the preparation of roof tiles shows that maximum MORs of 7.2 and 10.2 Mpa were obtained using 22% nickel slag and 40% aluminium slag, respectively, firing being carried out in both cases at 1100°C.

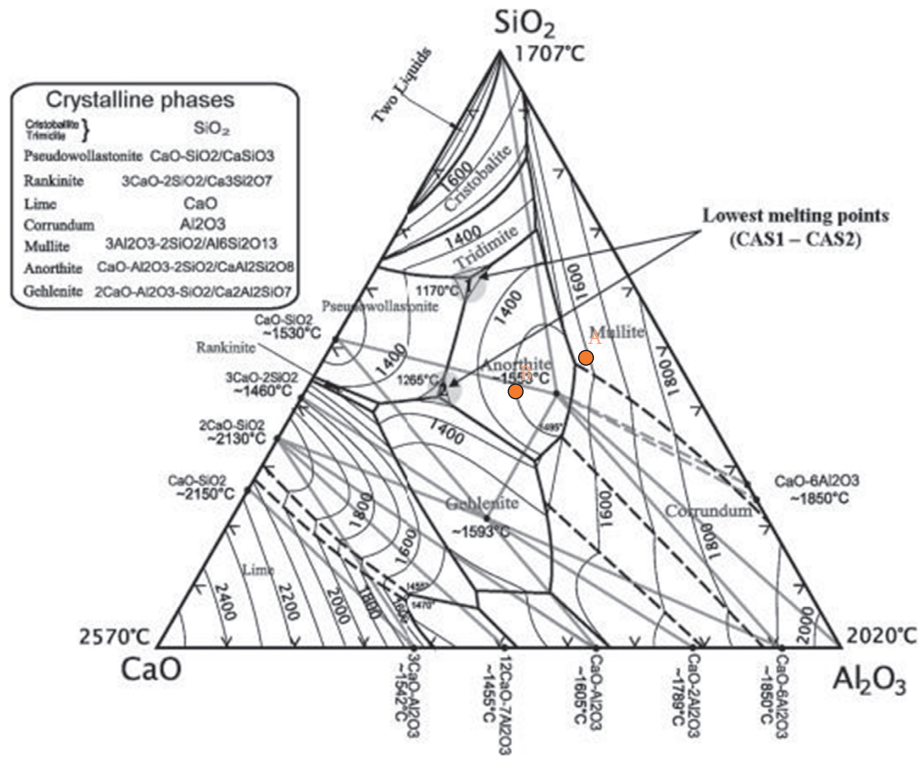

Figure 12: The SiO_2-Al_2O_3-CaO phase diagram [37].

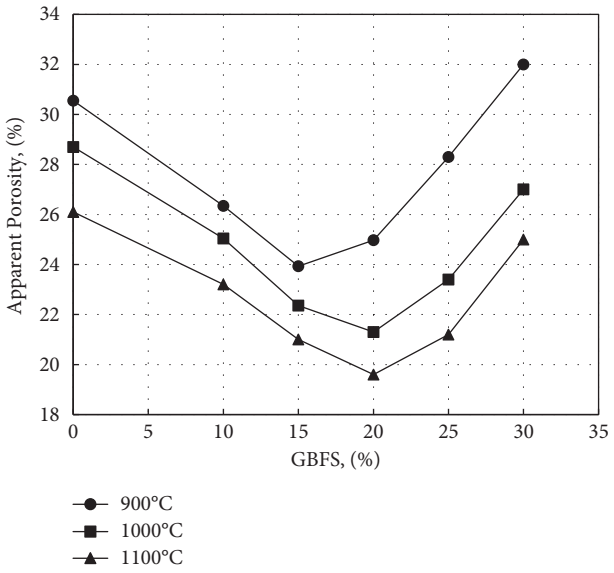

Figure 13: Effect of GBFS addition on apparent porosity.

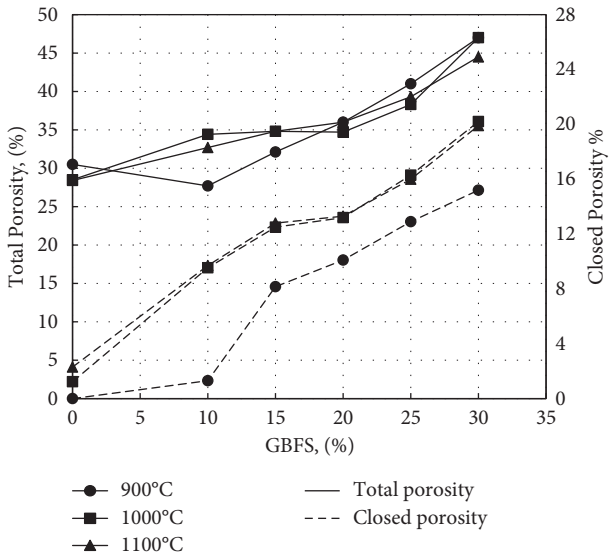

Figure 14: Effect of GBFS addition on total and closed porosity.

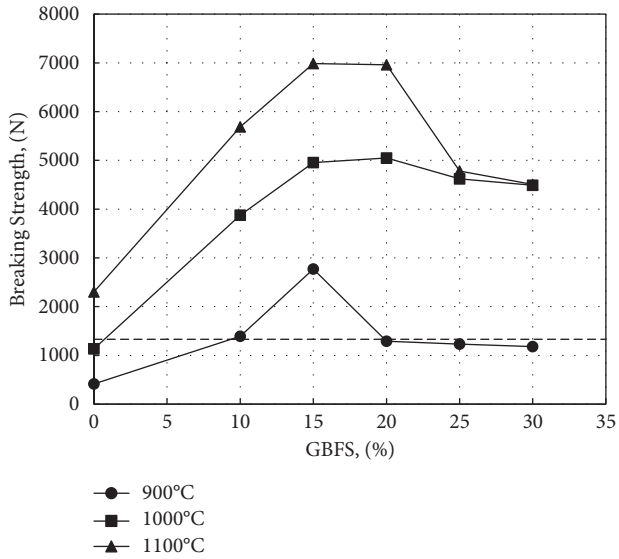

Figure 15: Effect of GBFS Addition on breaking strength. (Dotted line corresponds to minimum value following ASTM C1167).

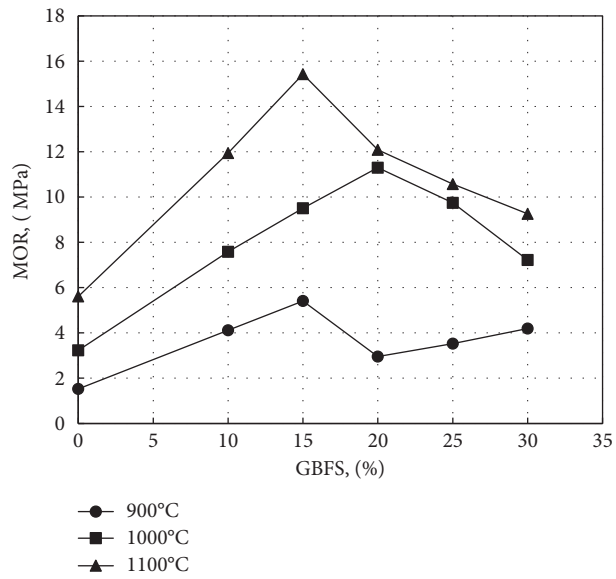

Figure 16: Effect of GBFS Addition on MOR.

Table 3: Comparison between the properties of the suggested sample and standard values.

Property	20% BFGS fired at 1000°C	20% BFGS fired at 1100°C	Standard values
Cold water absorption %	12.40	11.62	13
Saturation coefficient	0.82	0.75	0.86
Breaking Strength, N	5040	6950	1330
50 thawing-freezing cycles	Passes	Na*	Passes

*Freeze-thawing tests were not carried out for samples fired at 1100°C, although they would have almost certainly passed the test because of their superior properties over those fired at 1000°C.

4. Conclusion

The use of Blast Furnace Granulated Slag (BFGS) in the preparation of clay roof tiles was investigated by replacing the original mix with slag in percentages reaching 30%. The clay-waste mixes were formed by moulding, followed by drying and subsequent firing at three different temperatures, namely, 900°C, 1000°C, and 1100°C, for one hour.

An increase in the level of substitution of waste slag for clay resulted in a decrease in firing shrinkage so that samples containing more than 20% slag displayed an increase in volume, presumably due to bloating owing to excessive liquid phase formation and the expansion of trapped gases in pores. This has also caused cold water absorption to increase as the percent BFGS addition exceeds 20%. Samples fired at 1000°C and 1100°C containing 20% BFGS displayed a cold water absorption and a saturation coefficient below the maximum allowed values following ASTM C1167-03.

All samples fired at 1000°C and 1100°C with percent BFGS varying from 0% to 30% showed a transversal breaking strength exceeding the minimum standard value of 1330°N. Also, samples containing up to 20% BFGS fired at 1000°C successfully passed the freeze-thawing test, developing no cracks or fissures after 50 cycles.

A comparison between the properties of samples containing 20% BFGS and fired at 1000°C and 1100°C with the corresponding values for ASTM C1167-03 for normal duty roof tiles (grade 3) is summarized in Table 3.

To conclude, roof tiles can be manufactured with a standard clay mix (80%) and BFGS (20%) firing at 1000°C, with the produced tiles abiding by ASTM 1167-03 standards. The choice of a firing temperature of 1000°C rather than 1100°C is for obvious economic reasons.

Data Availability

All data are available in this article.

Conflicts of Interest

The authors declare that they have no conflicts of interest or personal relationships that could have appeared to influence the work reported in this paper.

References

[1] World Health Organization, *Chrysotile Asbestos*, WHO Publications, Geneva, Switzerland, 2014.

[2] S. Chiewnantawong, "[Townhouse design with energy efficiency]," *Master of Architecture Thesis*, Chulalongkorn University, Bangkok, Thailand, 2004.

[3] T. E. Omoniyi and B. A. Akinyemi, "Durability based suitability of bagasse-cement composite for roofing sheets," *Journal of Civil Engineering and Construction Technology*, vol. 3, no. 11, pp. 280–290, 2012.

[4] A. Franzblau, A. H. Demond, S. K. Sayler, H. D'Arcy, and R. L. Neitzel, "Asbestos-containing materials in abandoned residential dwellings in Detroit," *Science of the Total Environment*, vol. 714, Article ID 136580, 2020.

[5] "Environmentally Responsible," 2022, https://tileroofing.org/why-tile/environmental-impact/.

[6] M. Dondi, G. Guarini, M. Raimondo, and C. Zanelli, "Recycling PC and TV waste glass in clay bricks and roof tiles," *Waste Management*, vol. 29, no. 6, pp. 1945–1951, 2009.

[7] R. Gaggino, M. J. Positieri, P. Irico, J. Kreiker, R. Arguello, and M. P. A. Sánchez, "Ecological roofing tiles made with rubber and plastic wastes," *Advanced Materials Research*, vol. 844, pp. 458–461, 2013.

[8] M. S. Sultana, A. N. Ahmed, M. N. Zaman, M. A. Rahman, P. K. Biswas, and P. K. Nandy, "Utilization of hard rock dust with red clay to produce roof tiles," *Journal of Asian Ceramic Societies*, vol. 3, no. 1, pp. 22–26, 2015.

[9] D. Ingunza, M. Del Pilar, L. A. Dantas, and N. R. Maribondo, "Use of sewage sludge as raw material in the manufacture of roofs," in *Proceedings of the 2nd International Conference on Civil, Materials and Environmental Sciences*, pp. 31–33, London, UK, 2015.

[10] G. S. De Silva and M. L. Surangi, "Effect of waste rice husk ash on structural, thermal and run-off properties of clay roof tiles," *Construction and Building Materials*, vol. 154, pp. 251–257, 2017.

[11] A. K. Figen, Ö. Ünal, and S. Pişkin, "Manufacturing and characterization of roof tiles a mixture of tile waste and coal fly ash," *Süleyman Demirel Üniversitesi Fen Bilimleri Enstitüsü Dergisi*.vol. 21, no. 1, pp. 224–229, 2017.

[12] G. A. Khater, B. S. Nabawy, A. El-Kheshen, and M. A. Abdel-Latif, "Farag MM "use of arc furnace slag and ceramic sludge for the production of lightweight and highly porous ceramic materials" mater," *Baseline*, vol. 15, no. 3, 2022.

[13] F. P. E. Kallas, O. R. K. Montedo, and M. D. d M. Innocentini, "Use of nickel slag as raw material for roof tiles production," *Materials Science Forum*, vol. 912, pp. 212–217, 2018.

[14] S. K. Amin, S. A. El-Sherbiny, H. H. Abo-Almaged, and M. F. Abadir, "Recycling of marble waste in the manufacturing of ceramic roof tiles," *Waste Valorisation and Recycling*, Springer, Singapore, 2017.

[15] P. N. Lemougna, J. Yliniemi, E. Adesanya, P. Tanskanen, P. Kinnunen, and J. Roning, "Illikainen M "Reuse of copper slag in high-strength building ceramics containing spodumene tailings," *As Fluxing Agent" Minerals Engineerings*, vol. 155, Article ID 106448, 2020.

[16] M. M. Ahmed, M. F. Abadir, A. Youssef, and K. El-Naggar, "The use of aluminum slag waste in the preparation of roof tiles," *Master Research express*, vol. 8, Article ID 155201, 2021.

[17] H. Paiva, F. Simões, H. Maljaee, J. Yliniemi, M. Illikainen, and V. M. Ferreira, "Production of ceramic construction materials as an environmental management solution for sulfidic mine tailings," *SN Applied Sciences*, vol. 3, no. 8, p. 751, 2021.

[18] S. Ghosh, M. Das, S. Chakrabarti, and S. Ghatak, "Development of ceramic tiles from common clay and blast furnace slag," *Ceramics International Series*, vol. 28, no. 4, pp. 393–400, 2001.

[19] S. H. Kim, S. I. Kang, S. H. Kim, and J. H Kim, "The effect of anastomotic leakage on the incidence and severity of low anterior resection syndrome in patients undergoing proctectomy: a propensity score matching analysis," *Annals of coloproctology*, vol. 37, no. 5, pp. 281–290, 2021.

[20] L. Sidjanin, J. Ranogagec, D. Rajnovic, and E. Molnar, "Influence of firing temperature on mechanical properties on roofing tiles," *Mater and Design*, vol. 28, no. 3, pp. 941–947, 2007.

[21] ASTM C1167-03, *Standard Specification for Clay Roof Tiles*, ASTM International, West Conshohocken, PA, USA, 2003.

[22] ASTM C136-01, *Standard Test Method for Sieve Analysis of Fine and Coarse Aggregates*, ASTM International, West Conshohocken, PA, USA, 2017.
[23] ASTM C326-09, *Standard Test Method for Drying and Firing Shrinkages of Ceramic Whiteware Clays*, ASTM International, West Conshohocken, PA, USA, 2018.
[24] ISO 10545, *Ceramic Tiles-Determination of Water Absorption, Apparent Porosity, Apparent Relative Density and Bulk Density*, British Standards Institution Standards, London, UK, 2018.
[25] ISO 787-10, *General methods of test for pigments and extenders-Part 10: Determination of density-Pyknometer method*, International Organization for Standardization, Geneva, Switzerland, 1993.
[26] D. B. Rorabacher, "Statistical treatment for rejection of deviant values: critical values of Dixon's Q parameter and related subrange ratios at the 95% confidence level," *Analytical Chemistry*, vol. 63, no. 2, pp. 139–146, 1991.
[27] H. El Chabib, "Properties of Self Compacting Concrete with supplementary cementing materials," *Self Compacting Concrete: Materials, Properties and Applications*, vol. 13, pp. 283–308, 2020.
[28] S. A. T. Redfern, "The kinetics of dehydroxylation of kaolinite," *Clay Minerals*, vol. 22, no. 4, pp. 447–456, 1987.
[29] H. Goto and Y. Kakita, "Determination of free lime in slag," *Science Reports of Research Institutes, Tohoku University Series A Physics, Chemistry and Metallurgy*, vol. 7, pp. 135–139, 1955.
[30] E. Vilciu, M. Nicolae, and Nicolae, "A Minimization of the calcium oxide content in the steel slag, to be used in road construction," *U.P.B. Scientific Bulletin B*, vol. 73, no. 2, pp. 205–220, 2011.
[31] A. Cerato and A. J. Luttenegger, "Shrinkage of clays process," in *Proceedings of the 4th International Conference on Unsaturated Soils*, Phoenix, Arizona, 2006.
[32] Q. A. Saleh and B. F. Hassen, "Effect of CaO addition on the sintering behavior and microstructure of stoichiometric spinel," *International Journal of Physics*, vol. 5, no. 2, pp. 57–62, 2017.
[33] I. Ozdemir and S. Yilmaz, "Processing of unglazed ceramic tiles from blast furnace slag," *Journal of Materials Processing Technology*, vol. 183, no. 1, pp. 13–17, 2007.
[34] E. Kłosek-Wawrzyn, J. Małolepszy, and P. Murzyn, "Sintering behavior of kaolin with calcite," *Procedia Engineering*, vol. 57, pp. 572–582, 2013.
[35] S. Ghosh, M. Das, S. Chakrabarti, and S. Ghatak, "Development of ceramic tiles from common clay and blast furnace slag," *Ceramics International*, vol. 28, no. 4, pp. 393–400, 2002.
[36] O. Kovtun, I. Korobeinikov, A. K. Shukla, A. K. Shukla, and O. Volkova, "Viscosity of BOF slag," *Metals*, vol. 10, no. 7, p. 982, 2020.
[37] H. Mao, M. Hillert, M. Selleby, and B. Sundman, "Thermodynamic assessment of the CaO-Al_2O_3-SiO_2 system," *Journal of the American Ceramic Society*, vol. 89, no. 1, pp. 298–308, 2006.